The work function of doped polyaniline nanoparticles observed by Kelvin probe force microscopy

2012 Nanotechnology 23 365705

(http://iopscience.iop.org/0957-4484/23/36/365705)

Nanotechnology **23** (2012) 365705 (7pp) doi:10.1088/0957-4484/23/36/365705

The work function of doped polyaniline nanoparticles observed by Kelvin probe force microscopy

Jinsung Park[1,4], Doyeon Bang[2,4], Kuewhan Jang[1], Seungjoo Haam[2], Jaemoon Yang[3] and Sungsoo Na[1]

[1] Department of Mechanical Engineering, Korea University, Seoul 136-701, Korea
[2] Department of Chemical and Biomolecular Engineering, Yonsei University, Seoul 120-749, Korea
[3] Department of Radiology, College of Medicine Yonsei University, Seoul 120-752, Korea

E-mail: 177hum@yuhs.ac and nass@korea.ac.kr

Received 3 May 2012, in final form 17 July 2012
Published 21 August 2012
Online at stacks.iop.org/Nano/23/365705

Abstract
The work function of polyaniline nanoparticles in the emeraldine base state was determined by Kelvin probe force microscopy to be ∼270 meV higher than that of similar nanoparticles in the emeraldine salt state. Normal tapping mode atomic force microscopy could not be used to distinguish between the particles due to their similar morphologies and sizes. Moreover, other potential measurement systems, such as using zeta potentials, were not suitable for the measurement of surface charges of doped nanoparticles due to their encapsulation by interfering chemical groups. Kelvin probe force microscopy can be used to overcome these limitations and unambiguously distinguish between the bare and doped polyaniline nanoparticles.

(Some figures may appear in colour only in the online journal)

1. Introduction

Conducting polymers have attracted immense attention since a considerable conductance was discovered in these materials. Because of the low cost and flexibility in electronic applications, conducting polymers are candidate replacements for conventional metals and inorganic semiconductors [9, 12, 17, 33]. Polyaniline (PANI), a representative conducting polymer, has remarkable electrical conductivity that can be varied upon protonation or oxidation [31], and is one of the most technologically important polymers. In this regard, it has been widely used in printed circuit boards, electrochromic applications, protection against corrosion, and transparent conductive coatings [1, 7, 17]. Its nanoparticles are also subjected to much research: Lu *et al* reported that hybrid networks of PANI nanoparticles (PANPs) and carbon nanotubes could be used in vapor sensors [20]. In addition, PANPs are biocompatible, allowing them to be used in the study of cellular proliferation [4, 10]. Yang *et al* reported the possibility of using doped PANPs as near-infrared photothermal agents for reaction [35]. Despite their varied applicability, PANPs' basic electrical characteristics have not been fully elucidated [28]. Furthermore, for the general analysis and examination of doped or dedoped PANI application such as in semiconductor [34] and conductive coating [15, 17], a rapid and precise distinction technique is necessary with nanoscale resolution.

In this paper, we report an approach for identifying the work functions of individual PANPs at single-nanoparticle level using Kelvin probe force microscopy (KPFM). The foundations of KPFM lie in the work of Kelvin [13] and it is now widely used to analyze various materials such as metals [18, 25, 26] and biomaterials [16, 27, 30]. KPFM is a tool for measuring the local contact potential difference between a tip and the sample, by imaging the work function or surface potential of the sample with high

[4] These authors contributed equally to this work.

spatial resolution, and even subnanometer resolution [3, 22]. Moreover, the state of the art for KPFM measurement has reached the charge distribution within single molecules and between molecules [23]. The KPFM technique has already been demonstrated as an influential instrument for measuring electrostatic forces and the distributions of electric potentials with nanosize resolution [3, 19, 22], even to the single-molecule level [27, 29]. For example, Nam *et al* measured the surface potential of polymer patterned polypyrrole nanowire by KPFM [24]. Filleter *et al* measured local work functions of epitaxial graphene, finding variation between the results from single and double layers [8]. The work function of magnesium oxide has also been measured by KPFM [5]. Nonetheless, to the best of our knowledge, there have been no attempts to assess work function differences at single-particle resolution [5, 8, 18, 24–26]. In this work, we have utilized KPFM to analyze PANI nanoparticles at single-particle resolution and to observe the variation of the work function caused by doping. This approach could help to provide fundamental insight into conducting polymer application and discriminate between doped and dedoped PANPs with fast and precise measurements in ambient conditions, which opens new avenues for KPFM, offering a fiducial point of doped polymer application.

2. Experimental section

2.1. Polyaniline synthesis

Emeraldine base polyaniline (EB) was synthesized by chemical oxidation polymerization in the presence of excess hydrochloric acid. 0.2 mol aniline monomer was introduced in to 300 ml 1 M aqueous hydrochloric. Polymerization was conducted by the dropwise addition of 0.05 mol ammonium persulfate into 200 ml 1 M aqueous hydrochloric oxidant for 6 h at 4 °C. The precipitated polymer salt was recovered from the reaction vessel by filtration and re-dispersed in 500 ml 1 M sodium hydroxide. The deprotonated EB was then filtrated and re-dispersed in 500 ml acetone. Finally, fine EB powder was obtained after filtration and drying in a vacuum oven for 48 h.

Water soluble polyaniline nanoparticles were prepared by dissolving 10 mg EB powder in 4 ml chloroform. This organic phase was added to 20 ml aqueous phase containing 600 mg polyoxyethylene stearate. After mutual saturation of the organic and continuous phases, the mixture was emulsified for 10 min by 190 W ultrasonication (Sae Han SH-2100, Korea). After evaporation of the organic solvent, EB PANPs were purified by centrifugation (15 000 rpm for 30 min). The precipitated EB PANPs were dispersed in water phase until used. The prepared EB PANPs' absorbances were measured by absorption spectrometry (Mecasys UV-2120, Korea). The sizes and zeta potentials of particles were measured by laser scattering (ELS-Z, Otsuka Electronics, Japan).

2.2. Tapping mode AFM imaging

Tapping mode (or intermediate mode) AFM measurements were performed on an Innova (Veeco Corp., Santa Barbara, CA, USA) with a Nanodrive controller (Veeco, Santa Barbara, CA, USA) and closed-loop scanner in air at ambient temperature and pressure. The tapping mode, also represented as the amplitude modulation (AM) mode [22], was used to obtain clear images of polyaniline nanoparticles. In the tapping mode, the tip–sample interaction was altered as the tip–sample distance changed, leading to a change in oscillation amplitude. This closed-loop system confirmed the precise height profiles for each sample. The SCM-PIT cantilever tip was used for recording all images. The resonant frequency of this cantilever was 75 kHz and the tip radius was ∼20 nm. The cantilever was coated with Pt/Ir, for applying voltage. All image sizes were from 1 μm × 1 μm to 10 μm × 10 μm with scanning at 0.8 Hz. All images were leveled in two dimensions and processed with SPM Lab Analysis software V7.00 (Veeco Corp., Santa Barbara, CA, USA).

2.3. KPFM imaging

Generally, KPFM has two categories, such as a lift mode and a dual-frequency mode. The dual-frequency mode includes the amplitude modulation (AM) and frequency modulation (FM) modes [22]. The lift mode is a basic KPFM measurement method which is used for small potential variations (<100 mV) [27, 30]. In this experiment, the lift mode was used to detect the small polyaniline nanoparticles clearly. The tip bias potential oscillated at the same resonance frequency as the cantilever (∼75 kHz) used for acquiring the images. A three-step tuning procedure was applied prior to the KPFM imaging. The first step involved finding a clear image of a nanoparticle using the normal tapping mode with the same cantilever. To obtain a clear tapping mode image, we have adjusted tapping mode feedback parameters such as the proportional, integral and derivative gains. After getting a clear tapping mode image, the *y*-axis direction was then fixed and only the *x*-axis direction was analyzed with the same height profile as the sample. After obtaining repeated uniform profiles, we tried to find the lock-in phase parameter which is a dominant factor for KPFM measurement using a trial and error method. The lock-in phase must be adjusted to maximum contract, which is optimum for driving the potential feedback. After finding the optimum value of the lock-in phase, the KPFM parameters (proportional and integral corner frequency and overall gain) were finally set for the experiment. The fine-tuning of the KPFM control feedback parameter was through checking the KPFM ('SEPM' in our software version) error profile. The KPFM feedback parameters were most easily found by finding the value that gives minimum contrast in the KPFM error profile. The basic error range of KPFM is about ±10 mV. The average range of the error profile was checked and was stable below ±10 mV, implying accurate KPFM imaging. The tip was 100 nm above the surface. This is a suitable lift height which minimizes the interference between the tip and the sample. Also 4 V of alternating current (AC) amplitude was applied to the tip. The sample was grounded using a carbon tape and silver paste (Dotite, Japan). This grounded system helps reduce the error signal and reduces charge build-up phenomena in the various

pieces of equipment such as the scanning electron microscope. To maximize reliability, the same cantilever was used for each sample (EB and ES). Experiments were repeated using at least two different cantilevers. For avoiding tip wear, which was able to affect the KPFM measurement, we have prepared three protection methods. The first method was the Pt/Ir cantilever coating one. The iridium alloy was used to increase the durability of the coating [2]. The second method was the lift mode one, which reduces the tip abrasion because of tip and sample separation [27]. The last method was a tuning procedure for KPFM. The fixed *y*-axis image showed the tip sturdiness or tip wear from the uniform image or modified image. From these protection methods, we maintained the uniform KPFM images for the samples.

2.4. The physical concept of KPFM

KPFM is based on the work of Lord Kelvin [13] who first proposed the method for measuring the work function (i.e. surface potential) differences between two different materials. The basic definition of the contact potential, which is related to the difference in work function, is outlined here. The contact potential difference (CPD) between two materials—a KPFM tip and a sample—is defined as [14, 29]

$$V_{\mathrm{CPD}} = \frac{\phi_{\mathrm{sample}} - \phi_{\mathrm{tip}}}{q}, \tag{1}$$

where ϕ_{tip} and ϕ_{sample} are the work functions of the KPFM tip (i.e. platinum in this work) and the sample, respectively, and q is the elementary charge. A simple approximation of the force, F, between the tip and sample, is the electrostatic force between them:

$$F = \left.\frac{\partial E}{\partial z}\right|_Q = -\frac{1}{2}\Delta V^2 \frac{\partial C}{\partial z}, \tag{2}$$

where the electrostatic energy, E, is that of a parallel plate capacitor: $E = \frac{1}{2}C\Delta V^2$ with C being the tip–sample capacitance, z the distance between the tip and sample, and ΔV the potential difference between the two capacitor plates. Inserting the following equation for the potential difference: $\Delta V = V_{\mathrm{DC}} - V_{\mathrm{CPD}} + V_{ac}\sin(\omega t)$ where V_{DC} is a nullifying voltage applied in order to measure the CPD, into equation (2), we obtain

$$F = \left.\frac{\partial E}{\partial z}\right|_Q = -\frac{1}{2}\frac{\partial C}{\partial z}\left[(V_{\mathrm{DC}} - V_{\mathrm{CPD}})^2 + \frac{1}{2}V_{ac}^2\right] - \frac{\partial C}{\partial z}(V_{\mathrm{DC}} - V_{\mathrm{CPD}})V_{ac}\sin(\omega t) + \frac{1}{4}\frac{\partial C}{\partial z}V_{ac}^2\cos(2\omega t). \tag{3}$$

Here, equation (3) is composed of three parts: the DC term, the ω term and the 2ω term. The cantilever responds only to forces at or very near its resonance, so the DC and 2ω terms do not cause any significant oscillation of the cantilever. In terms of a frequency, ω, we have

$$F_\omega = \frac{\partial C}{\partial z}(V_{\mathrm{CPD}} - V_{\mathrm{DC}})V_{ac}\sin(\omega t), \tag{4}$$

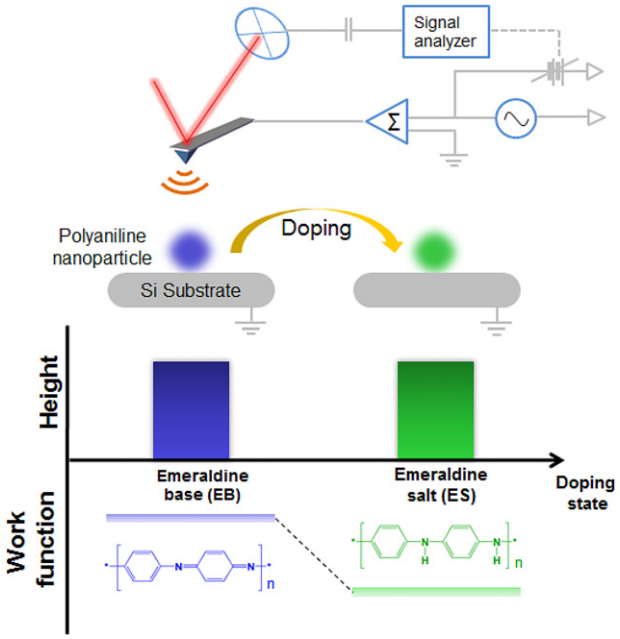

Figure 1. Measuring the electrical properties of polyaniline nanoparticles via Kelvin probe force microscopy in the emeraldine base state and the emeraldine salt state.

In general, KPFM measures the force exerted due to the surface potential difference, and the work function difference can be estimated from the physical concept depicted in equation (4).

3. Results and discussion

The sizes and work functions of PANPs were measured simultaneously by tapping mode atomic force microscopy (tmAFM) and KPFM (figure 1). Water soluble PANPs, synthesized in nanoemulsions, were dropped onto silicon substrates. Topographic heights and local work functions of the particles were then recorded. To compare the heights and work functions of emeraldine base polyaniline nanoparticle (EB PANPs) and emeraldine salt polyaniline nanoparticle (ES PANPs), 1 M aqueous HCl was used for doping the nanoparticles. The sizes of PANPs were not significantly altered by doping, though their local work functions decreased.

Bare PANPs are not appropriate for various applications, especially biological ones, due to their hydrophobicity and tendency to aggregate [35]. Therefore water soluble PANPs were synthesized and analyzed to demonstrate a potential use of monitoring individual particles. Polyaniline was synthesized using anilinium salt protonation by hydrochloride (HCl) and ammonium persulfate oxidant. Chemical oxidative polymerization was carried out for 6 h at 4 °C, resulting in dark green precipitates (ES) that were purified by washing with copious amounts of deionized water. The synthesized ES PANPs were dedoped using sodium hydroxide to increase the solubility of polyaniline in the organic phase (chloroform) and to obtain homogeneously sized nanoparticles. The color of the resulting powder was purple (EB). To increase the water

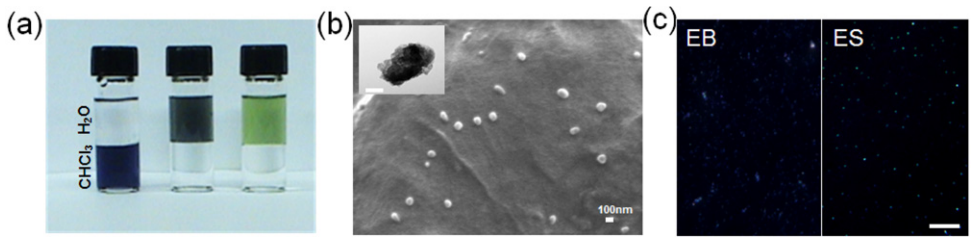

Figure 2. (a) Solubility tests of emeraldine base (left), EB PANP (middle) and ES PANP (right). The upper layer is aqueous and the lower layer is organic. (b) SEM images of EB PANP; inset, TEM image. The scale bar is 100 nm. The TEM scale bar is 50 nm. (c) Dark-field microscope image of EB PANP (left) and ES PANP (right).

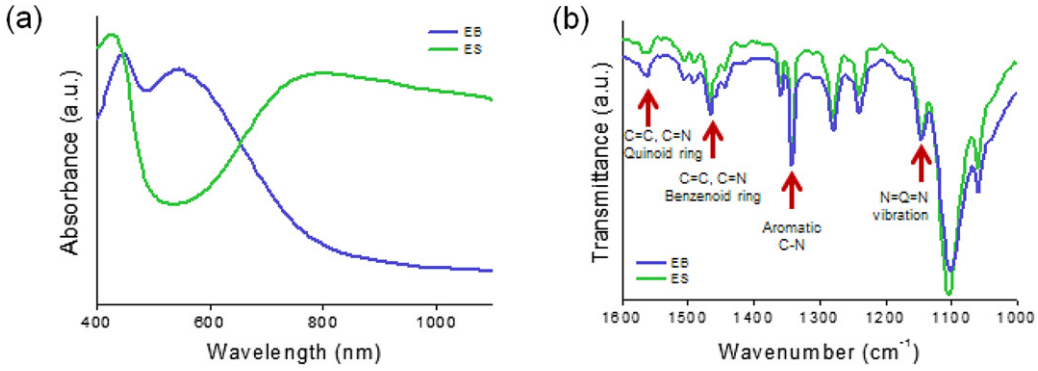

Figure 3. (a) UV–visible absorption spectrum; (b) FT-IR transmittance spectrum.

solubility of PANPs, they were synthesized in nanoemulsions by simultaneously encapsulating the hydrophobic EB PANPs with amphiphilic PEGylated fatty acid (polyethylene glycol stearate) in water. The EB PANPs were then doped in 1 M aqueous HCl to prepare ES PANPs. The hydrophobic EB PANP phase transferred to the hydrophilic EB PANPs or ES PANPs (figure 2(a)). EB was dissolved in the lower chloroform phase due to its innate hydrophobicity, whereas EB PANPs and ES PANPs dissolved in the upper water phase. This indicates that the PEGylated PANPs were highly water soluble due to their outer polyoxyethylene chains. Scanning electron microscopy (SEM) showed that the EB PANPs have smooth surfaces and narrow size distributions (figure 2(b)). Dark-field microscopy images of light scattered from individual EB PANPs and ES PANPs were recorded (figure 2(c)). White light from a 100 W halogen lamp was focused under large angles onto the samples using a dark-field condenser (NA = 1.2). The EB PANPs and ES PANPs scattered blue and green light, respectively. Moreover, the color change of the EB PANPs from blue to the green of the ES PANPs was attributed to the generation of inter-bandgap states by doping under acidic conditions [11]. The absorbance peak of polyaniline was red-shifted toward the NIR region as a result of its transition from the EB to the ES during the doping process (figure 3(a)). Furthermore, the chemical structure of PANPs (both EB and ES states) was confirmed using FT-IR spectra: 1148 cm^{-1} (N=Q=N vibrations), 1,330 cm^{-1} (aromatic C–N stretching), 1,467 cm^{-1} (C=C and C=N stretching of benzenoid rings) and 1563 cm^{-1} (C=C and C=N stretching of quinoid rings) from PANPs (figure 3(b)).

For the general approach of particle analysis, zeta potentials of PANPs were measured to assess their sizes and electrical potentials in the liquid state (figure 4). To measure the hydrodynamic radii and zeta potentials, 5 mg ml^{-1} aqueous PANPs were prepared. In figure 4(a), the hydrodynamic radius distribution followed the Mie scattering theory which presents the weight percentage using light scattering. The following equation is $v = (4/3)\pi r^2$. The average of hydrodynamic radii of EB PANPs (115.6 ± 16.3 nm) and ES PANPs (121.3 ± 23.4 nm) did not show any significant difference and had narrow size distributions. This implies that the average size of the PANPs was not changed by doping. Moreover, the electrical potential of ES PANPs was slightly lower than those of EB PANPs that belong to the error range (figure 4(b)). The zeta potentials of the EB PANPs and the ES PANPs were 2.1 ± 1.2 mV and 0.2 ± 2.1 mV, respectively. From the zeta potential data, we noticed that PANPs were shown to be a neutral state because of neutral PEG encapsulation. This shows that assessing zeta potentials cannot be used to provide electrical information about the PANPs coated with interference groups such as PEG. In other words, the zeta potentials are limited in distinguishing the state of particles despite the great electrical differences between the EB and ES states.

Due to the inapplicability of the zeta potential method for single and PEG coated PANPs, we have demonstrated the shape and work function difference of PANPs using tmAFM and KPFM. 5 mg ml^{-1} PANP samples were diluted with deionized water to concentrations from 5 μg ml^{-1} to 5 ng ml^{-1}. From each concentration, 2 μl polyaniline solutions were dispensed onto silicon substrates, dried

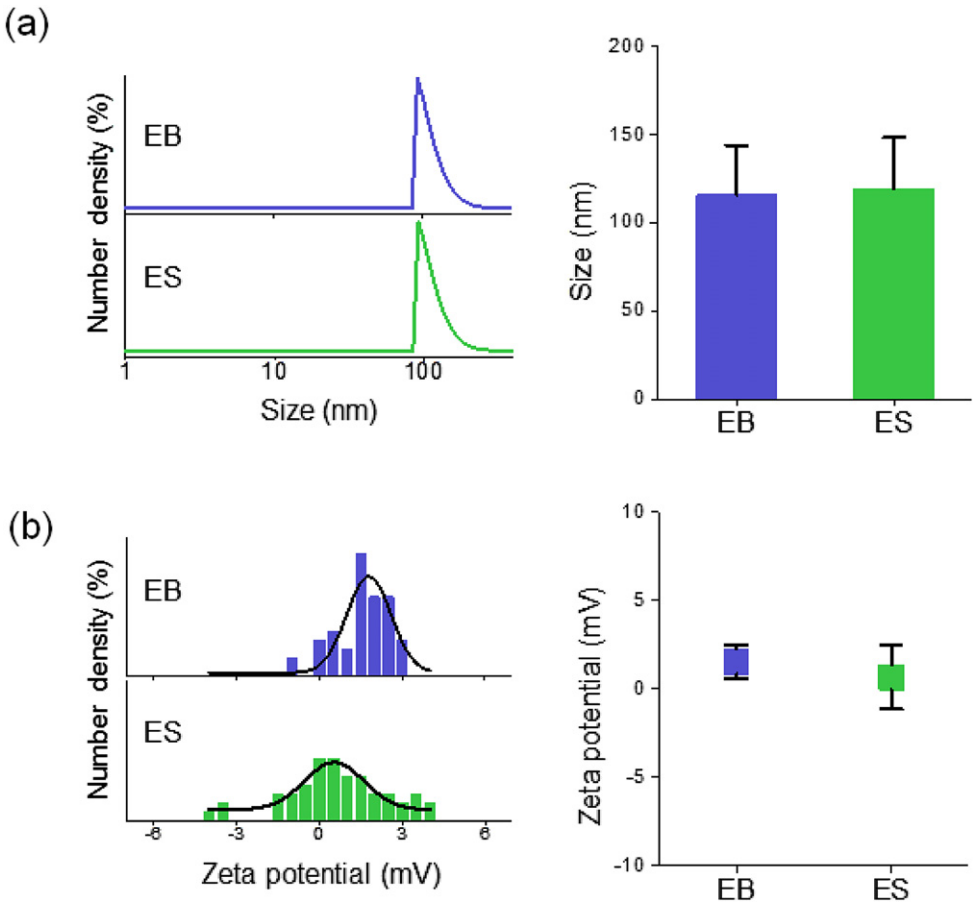

Figure 4. (a) Hydrodynamic radius distributions and averages for EB PANP (blue) and ES PANP (green). (b) Zeta potentials of EB PANP (blue) and ES PANP (green).

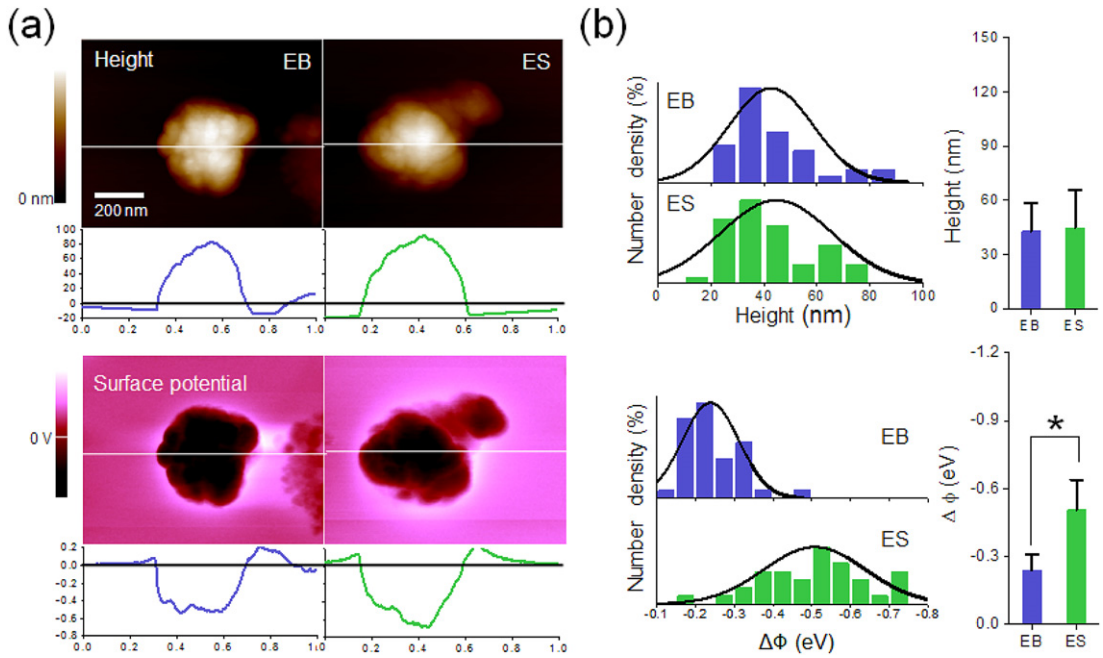

Figure 5. (a) Electrical property mapping of a single EB PANP (left) and ES PANP (right). Line profiles of each image are depicted below. (b) Distribution and average of height and work function differences between EB PANP and ES PANP measured by tmAFM and KPFM, respectively ($n > 50$, $^*p < 0.0001$).

overnight under vacuum, and tmAFM and KPFM were then conducted. Among these concentrations, 5 ng ml^{-1} (0.01 ng) showed the best result as regards an individual particle image (figure 5(a)). For measuring and statistical analysis, the heights and work functions of the samples were assessed (figure 5(b)), for over 50 individual PANPs in each case. The tapping mode images and size distributions showed that the heights of EB PANPs (42.77 ± 15.8 nm) and ES PANPs (44.74 ± 21.1 nm) were similar despite the doping. It is noteworthy that the heights of both EB PANPs and ES PANPs were around 50 nm and their lateral sizes were around 300 nm in tmAFM images (figure 5(b)). There were three significant points as regards PANP height measurement using tmAFM. The first was the irregular shape of the PANPs. As seen in the SEM image of a PANP sample in figure 2(b), not all PANPs were spherically shaped. This was due to the fact that the solubility of polyaniline was slightly poor in chloroform and a compact coil conformation is presented [21]. Therefore, PANPs had the possibility of an irregular surface which led to one-axis long shapes. The polyaniline containing chloroform droplets took on one-axis long shapes as the chloroform dried during the nanoemulsion process. The sizes of PANPs seen from the SEM or TEM images (around 120 nm) in figure 2(b) were comparable with the hydrodynamic radii (around 120 nm) in figure 4(a). Second, the surfactant of the PANPs had the possibility of increasing the lateral size for AFM. In the liquid state, the PEG molecules were inflated. However, in the dry state, surfactants shrank and drooped on each side of the nanoparticles. These drooped surfactants were able to increase the lateral size of dried PANPs. The third point is an artifact of AFM imaging. During the imaging, two major AFM artifacts could appear. The first one was a profile broadening effect due to the tip and sample convolution. The second one was a height lowering effect due to the elastic deformation of sample objects [32]. In our case, PANPs were coated with PEG which was more flexible than the tip. So both artifacts could affect the tapping mode images. Since the size of the particles was smaller than the AFM tip size (the tip radius is 20 nm, with 25° for the tip angle), distortion of the lateral image was induced. Therefore, smaller height was induced due to the irregular shape of the PANPs, the drooped surfactant of the PANPS and AFM artifacts. As a result of KPFM, the polyaniline nanoparticles showed a negative surface potential (figure 5) because the work function of the polyaniline nanoparticles was lower than that of platinum (the work function of Pt is 6.1 ± 0.06 eV) [6] for a surface of the KPFM cantilever (see section 2). In contrast to the height distribution of the PANPs, an obvious work function difference ($\Delta\Phi$) was observed by KPFM between the EB PANPs ($\Delta\Phi = -239.3 \pm 71.9$ meV) and the ES PANPS ($\Delta\Phi = -507.4 \pm 131.1$ meV) (figure 5(b)). Doping reduced the work function of the ES PANPs to about ~270 meV below that of the EB PANPs. In addition, we analyzed the statistical T-test, which is able to distinguish the dependent (paired) and independent (unpaired) samples. Generally, the value of p is smaller than 0.01; all samples are independent samples. In our case, the value of p is smaller than 0.0001, which also validated the significance of the difference between EB and ES PANPs ($^*p < 0.0001$).

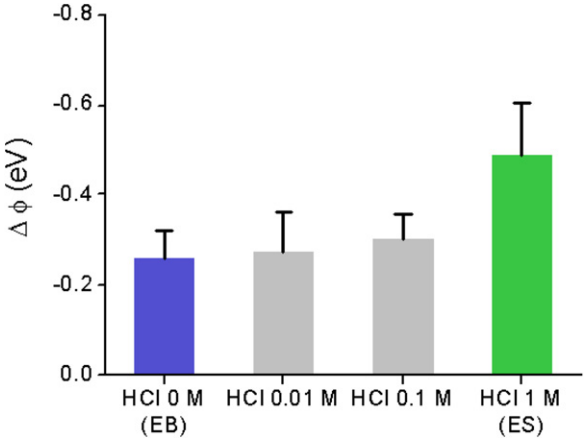

Figure 6. Electrical properties of single PANPs with respect to HCl concentration; HCl is the doping agent ($n > 50$).

We have also measured the difference in work function with respect to the HCl concentration using KPFM ($n > 50$). As mentioned before, HCl was a doping agent which induced EB PANPs from ES PANPs. In figure 6, from 0 (pH 7.4, EB PANPs) to 0.1 M of HCl concentration, the averages of $\Delta\Phi$ increase exiguously. Specifically, the work function differences for 0.01 M (<pH 3) and 0.1 M (pH 2) of HCl are −271.7±66.5 meV and −301.5±50.6 meV, respectively. This result showed that the increment of $\Delta\Phi$ was below the error range. However, 0.1 M and 1 M (pH 1, ES PANPs) of HCl depicted clearly the distinction between the work function differences. This graph showed a similar result to previous research which dealt with the UV absorption ratio to the pH, to clarify the PANP situation in the bulk state [26]. These results show that the doped state of the polyaniline nanoparticles was distinguishable through the differences in work function observed by KPFM with single-particle resolution.

4. Conclusion

In summary, we have found that the work function differences of individual polyaniline nanoparticles could be observed using KPFM. Our study showed that the zeta potential method was not suitable for distinguishing between the states of PEGylated polyaniline nanoparticles because the zeta potential only concerns the covering surface charge of nanoparticles and the charge of particles is dominantly affected by the neutral charge of PEG. Likewise, owing to EB and ES PANPs having the same height, tmAFM was not an appropriate approach for discrimination. On the other hand, KPFM could be used to distinguish between the two states of the PANPs through assessing the differences of their work functions. In conclusion, our study could not only indicate a generalized distinguishable platform for doped conducting polymer but also present a new measurement system for polymer application in single-particle resolution. Moreover, it will be possible to investigate the charge distribution of single nanoparticles due to the further development of KPFM.

Acknowledgments

This work was supported by the National Research Foundation of Korea (NRF) under Grant Nos NRF-2012-

0000785 and NRF-2011-0020090, and the National Research Foundation of Korea funded by the Korean government (MEST) under Grant Nos 2010-0020648 and 2011-0026073.

References

[1] Anilkumar P and Jayakannan M 2006 New renewable resource amphiphilic molecular design for size-controlled and highly ordered polyaniline nanofibers *Langmuir* **22** 5952–7

[2] Balko E N and Nguyen P H 1991 Iridium–tin mixed oxide anode coatings *J. Appl. Electrochem.* **21** 678–82

[3] Barth C, Foster A S, Henry C R and Shluger A L 2011 Recent trends in surface characterization and chemistry with high-resolution scanning force methods *Adv. Mater.* **23** 477–501

[4] Bidez P R, Li S, MacDiarmid A G, Venancio E C, Wei Y and Lelkes P I 2006 Polyaniline, an electroactive polymer, supports adhesion and proliferation of cardiac myoblasts *J. Biomater. Sci. Polym. Edn* **17** 199–212

[5] Bieletzki M, Hynninen T, Soini T M, Pivetta M, Henry C R, Foster A S, Esch F, Barth C and Heiz U 2010 Topography and work function measurements of thin MgO(001) films on Ag(001) by nc-AFM and KPFM *Phys. Chem. Chem. Phys.* **12** 3203–9

[6] Derry G N and Ji-Zhong Z 1989 Work function of Pt(111) *Phys. Rev.* B **39** 1940–1

[7] Fehse K, Schwartz G, Walzer K and Leo K 2007 Combination of a polyaniline anode and doped charge transport layers for high-efficiency organic light emitting diodes *J. Appl. Phys.* **101** 124509

[8] Filleter T, Emtsev K V, Seyller T and Bennewitz R 2008 Local work function measurements of epitaxial graphene *Appl. Phys. Lett.* **93** 133117

[9] Guo S and Wang E 2008 Simple electrochemical route to nanofiber junctions and dendrites of conducting polymer *Langmuir* **24** 2128–32

[10] Heeger A J 2001 Halbleitende und metallische polymere: polymere materialien der vierten generation (Nobel-Vortrag) *Angew. Chem.* **113** 2660–82

[11] Heeger A J 2001 Semiconducting and metallic polymers: the fourth generation of polymeric materials (Nobel Lecture) *Angew. Chem. Int. Edn* **40** 2591–611

[12] Huang C, Lu N, Wang Y, Tian L, Yang B, Dong B and Chi L 2010 A simple method for the fabrication of high-resolution conducting polymer patterns *Langmuir* **26** 9142–5

[13] Kelvin L 1898 Contact electricity of metals *Phil. Mag.* **46** 82–120

[14] Kitamura S I and Iwatsuki M 1998 High-resolution imaging of contact potential difference with ultrahigh vacuum noncontact atomic force microscope *Appl. Phys. Lett.* **72** 3154–6

[15] Kwon J Y, Kim E Y and Kim H D 2004 Preparation and properties of waterborne-polyurethane coating materials containing conductive polyaniline *Macromol. Res.* **12** 303–10

[16] Leung C, Kinns H, Hoogenboom B W, Howorka S and Mesquida P 2009 Imaging surface charges of individual biomolecules *Nano Lett.* **9** 2769–73

[17] Lin Y-J, Yang F-M and Lin C-S 2007 Effects of ultraviolet irradiation on energy band structure and conductivity of polyaniline *J. Appl. Phys.* **102** 103702

[18] Liscio A, Palermo V and Samorí P 2008 Probing local surface potential of quasi-one-dimensional systems: a KPFM study of P3HT nanofibers *Adv. Funct. Mater.* **18** 907–14

[19] Liscio A, Palermo V and Samori P 2010 Nanoscale quantitative measurement of the potential of charged nanostructures by electrostatic and Kelvin probe force microscopy: unraveling electronic processes in complex materials *Acc. Chem. Res.* **43** 541–50

[20] Lu J, Park B J, Kumar B, Castro M, Choi H J and Feller J-F 2010 Polyaniline nanoparticle–carbon nanotube hybrid network vapour sensors with switchable chemo-electrical polarity *Nanotechnology* **21** 255501

[21] MacDiarmid A G and Epstein A J 1995 Secondary doping in polyaniline *Synth. Met.* **69** 85–92

[22] Melitz W, Shen J, Kummel A C and Lee S 2011 Kelvin probe force microscopy and its application *Surf. Sci. Rep.* **66** 1–27

[23] Mohn F, Gross L, Moll N and Meyer G 2012 Imaging the charge distribution within a single molecule *Nature Nano* **7** 227–31

[24] Nam K, Lee G, Jung H, Park J, Kim C H, Seo J, Yoon D S, Lee S W and Kwon T 2011 Single-step electropolymerization patterning of a polypyrrole nanowire by ultra-short pulses via an AFM cantilever *Nanotechnology* **22** 225303

[25] Palermo V, Liscio A, Palma M, Surin M, Lazzaroni R and Samori P 2007 Exploring nanoscale electrical and electronic properties of organic and polymeric functional materials by atomic force microscopy based approaches *Chem. Commun.* 3326–37

[26] Palermo V *et al* 2008 The relationship between nanoscale architecture and function in photovoltaic multichromophoric arrays as visualized by Kelvin probe force microscopy *J. Am. Chem. Soc.* **130** 14605–14

[27] Park J *et al* 2011 Single-molecule recognition of biomolecular interaction via Kelvin probe force microscopy *ACS Nano* **5** 6981–90

[28] Park S Y, Cho M S and Choi H J 2004 Synthesis and electrical characteristics of polyaniline nanoparticles and their polymeric composite *Curr. Appl. Phys.* **4** 581–3

[29] Rosenwaks Y, Shikler R, Glatzel T and Sadewasser S 2004 Kelvin probe force microscopy of semiconductor surface defects *Phys. Rev.* B **70** 085320

[30] Sinensky A K and Belcher A M 2007 Label-free and high-resolution protein/DNA nanoarray analysis using Kelvin probe force microscopy *Nature Nano* **2** 653–9

[31] Singh R, Arora V, Tandon R P, Chandra S and Mansingh A 1998 Charge transport and structural morphology of HCl-doped polyaniline *J. Mater. Sci.* **33** 2067–72

[32] Troyon M, Hazotte A and Bourhettar A 1994 Modeling the AFM tip effect for quantitative-analysis of precipitate volume fraction in nickel-based superalloys *Microsc. Microanal. Microstruct.* **5** 489–99

[33] Xu B, Ovchenkov Y, Bai M, Caruso A N, Sorokin A V, Ducharme S, Doudin B and Dowben P A 2002 Heterojunction diode fabrication from polyaniline and a ferroelectric polymer *Appl. Phys. Lett.* **81** 4281–3

[34] Yakuphanoglu F and Şenkal B F 2007 Electronic and thermoelectric properties of polyaniline organic semiconductor and electrical characterization of Al/PANI MIS diode *J. Phys. Chem.* C **111** 1840–6

[35] Yang J *et al* 2011 Convertible organic nanoparticles for near-infrared photothermal ablation of cancer cells *Angew. Chem. Int. Edn* **50** 441–4